

Article

Mathematical and Physical Characteristics of the Phase Spectrum of Earthquake Ground Motions

Yanqiong Ding ¹ , Yazhou Xu ¹ and Huiquan Miao ^{2,3,*}

¹ School of Civil Engineering, Xi'an University of Architecture and Technology, Xi'an 710055, China; dingyanqiong18@163.com (Y.D.); xuyazhou@xauat.edu.cn (Y.X.)

² Faculty of Architecture, Civil and Transportation Engineering, Beijing University of Technology, Beijing 100124, China

³ Key Laboratory of Urban Security and Disaster Engineering, China Ministry of Education, Beijing University of Technology, Beijing 100124, China

* Correspondence: miaohq@126.com

Abstract: This study presents a rigorous investigation into the mathematical and physical properties inherent in the Fourier phase spectrum of earthquake ground motions. This exploration includes a detailed examination of the probability distribution of phase angles and differences, elucidated through two novel numerical experiments utilizing the reduction ad absurdum approach. Moreover, the study scrutinizes the physical attributes of earthquake ground motion's phase spectrum, employing the circular frequency-dependent phase derivative as a key analytical factor. In a novel approach, the research delves into the relationship between circular frequency-dependent phase derivatives and Fourier amplitudes, shedding light on essential connections within earthquake phenomena, particularly addressing non-stationarity. Expanding the scope, the study comprehensively examines the influence of source, propagation path, and site on both the phase spectrum and accelerogram. Employing the control variate technique facilitates this analysis, providing valuable insights into the underlying physical mechanisms governing earthquake wave behavior. The findings highlight the temporal properties of the phase spectrum, attributing its complexity to the temporal heterogeneity in energy release during the fault rupture and dispersion of earthquake waves. This novel approach not only enhances the understanding of earthquake dynamics, but also underscores the significance of considering temporal variations in earthquake events.



Citation: Ding, Y.; Xu, Y.; Miao, H. Mathematical and Physical Characteristics of the Phase Spectrum of Earthquake Ground Motions.

Buildings **2024**, *14*, 1250. <https://doi.org/10.3390/buildings14051250>

Academic Editor: Humberto Varum

Received: 27 March 2024

Revised: 22 April 2024

Accepted: 26 April 2024

Published: 28 April 2024



Copyright: © 2024 by the authors. Licensee MDPI, Basel, Switzerland. This article is an open access article distributed under the terms and conditions of the Creative Commons Attribution (CC BY) license (<https://creativecommons.org/licenses/by/4.0/>).

Keywords: earthquake ground motions; phase spectrum; mathematical characteristics; physical characteristics; envelope delay

1. Introduction

The Fourier transform is very useful in the study of the characteristics of earthquake waves [1–3]. A real acceleration time history of the earthquake is transformed into an amplitude spectrum and a phase spectrum by applying the Fourier transform. The amplitude spectrum describes the distribution of the energy of the earthquake ground motion with frequency, whose shape is always regular. The models of the amplitude spectrum [4–6], as well as the famous models of the power spectrum, such as the Kanai–Tajimi spectrum [7,8] and the Clough–Penzien spectrum [9], seem to be adequate for the generation of earthquake ground motions. In contrast, the phase spectrum is more irregular owing to the periodicity of the phase angles.

Although significant attention has been paid to the importance of phase in some fields, e.g., in signal processing, image processing, and human speech recognition, even some research reveals that, in some situations, many of the important features of a signal are preserved if only the phase is retained [10–15]. Despite this, the phase spectrum appears to be undervalued within the realm of earthquake engineering. Progress in studying the phase spectrum in earthquake engineering has been sluggish. Typically, the phase angles

of earthquake ground motions are usually assumed to be independent and uniformly distributed random variables in the domain $[0, 2\pi]$ [16–20], a presumption drawn from statistical analyses of real accelerograms. However, this assumption of independent and uniformly distributed random phase angles results in time-stationary earthquake ground motions, which may not accurately reflect the true behavior of phase angles.

After Ohsaki [21] indicated that the phase difference appears to be normal or apparently normal, and its probability density function (PDF) is closely related to the wave shape of the earthquake ground motion, other studies focused on the probability distribution of the phase difference [22–28]. Furthermore, a specific distributed phase difference was used to simulate earthquake ground motions [29–36]. However, employing phase differences governed by specific distributions (such as normal and lognormal distributions) yields simulations with similar temporal shapes. Consequently, the stochastic nature of earthquake ground motion waveforms remains inadequately captured. This highlights the challenge of describing the intricate characteristics of the phase spectrum solely through mathematical formulations, disregarding their physical interpretations.

Furthermore, the relationship between the Fourier phase spectrum and the Fourier amplitude spectrum is of interest to earthquake engineering researchers. In a pioneering study conducted by Thráinsson and Kiremidjian, the phase difference was found to be contingent upon the Fourier amplitude [25]. On this basis, Boore introduced a circular frequency-dependent phase derivative (measured in time units) instead of the phase difference to investigate the relationship between the phase derivative and the Fourier amplitude, which revealed that the largest amplitudes occurred over a relatively narrow time range, whereas smaller amplitudes were spread out over the entire time range [37]. However, this outcome proved perplexing because the circular frequency-dependent phase derivative calculated by Boore [37] using continuous Fourier transform yielded a vastly different range compared to the duration of the accelerogram, including some negative values. In this regard, Ding et al. proposed a new method to calculate the circular frequency-dependent phase derivative based on the discrete Fourier transform to obtain the same range as the duration of the accelerogram and avoid negative values [38]. In this method, wave groups with larger amplitudes arrived at the same time when a strong shock occurred. Thus, from the brief outline of some major contributions to the relation of the phase spectrum and the Fourier amplitude, the time property of the phase spectrum was indicated. While recent studies have endeavored to model the phase characteristics of accelerograms using envelope delay [39,40] and group velocity dispersion curves [41], they have overlooked the relationship between phase and amplitude.

In this study, the mathematical characteristics of the phase angle and phase difference and the physical characteristics of the phase spectrum were studied. The subsequent sections of this paper are structured to unfold our investigation comprehensively. Section 2 delves into an exploration of the probability distributions governing phase angles and phase differences. Moving forward, Section 3 delves deeper into the physical interpretation of the phase spectrum, particularly through an analysis of the circular frequency-dependent phase derivative. This exploration lays the groundwork for understanding the relationship between the phase spectrum, amplitude, and duration, which is further expounded upon. In Section 4, we delve into elucidating the impact of various factors, such as source characteristics, propagation path, and site conditions, on the phase spectrum. Finally, in the concluding section, we synthesize our findings and offer conclusive remarks. This sequential arrangement not only facilitates a structured understanding of our research, but also underscores the interconnectedness of the various aspects explored throughout the study.

2. Mathematical Characteristics of the Phase Angles and Phase Differences

2.1. Probability Distribution of the Phase Angles

The discrete acceleration time history of earthquake ground motion, $a(t)$, can be expressed by a finite Fourier series:

$$a(t) = \sum_{k=0}^n A_k \cdot \cos(\omega_k t + \varphi_k) \quad (1)$$

where A_k is the Fourier amplitude, φ_k is the Fourier phase angle corresponding to ω_k , $\omega_k = 2\pi k/T$ is the circular frequency of the k th harmonic, T is the duration of the time history, $n = T/(2\Delta t)$, and Δt is the time increment of the time history. The phase difference angle, $\Delta\varphi_k$, is defined by Ohsaki [21] as follows:

$$\Delta\varphi_k = \varphi_{k+1} - \varphi_k, \quad (k = 1, 2, 3, \dots, n-1) \quad (2)$$

It is generally believed that the phase angle is uniformly distributed when all phase angles are in the domain $[0, 2\pi)$, as shown in Figure 1, and the phase difference follows a normal distribution, as shown in Figure 2. A wealth of earthquake ground motions support this conviction.

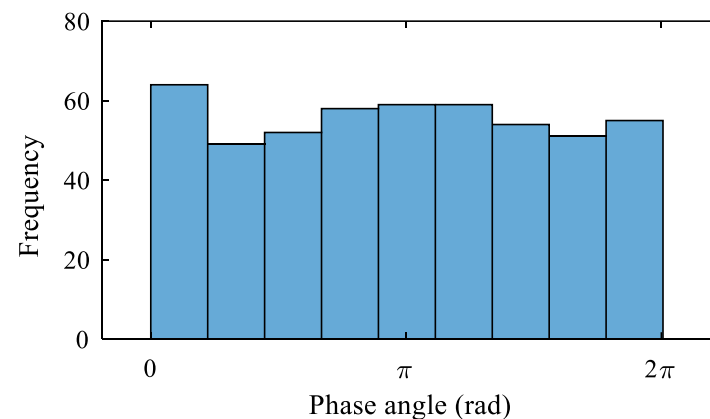


Figure 1. Typical frequency distribution of phase angles of a certain accelerogram.

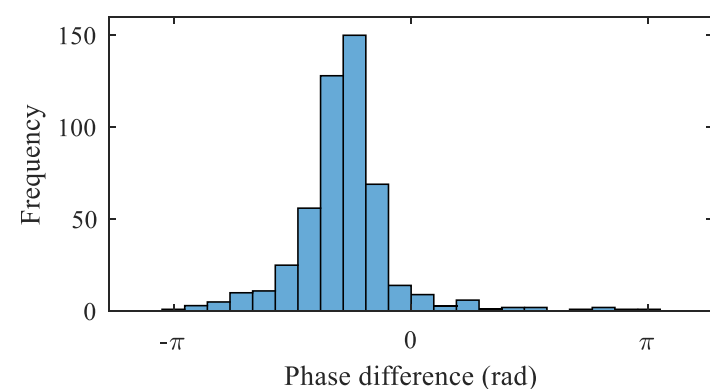


Figure 2. Typical frequency distribution of phase differences of a certain accelerogram.

The Fourier phase angles of earthquake ground motions are assumed to be independent and uniformly distributed random variables in the domain $[0, 2\pi)$, that is, $\varphi_k \sim U[0, 2\pi)$, $\varphi_{k+1} \sim U[0, 2\pi)$. PDFs $f_{\varphi_k}(\alpha)$ and $f_{\varphi_{k+1}}(\beta)$ of φ_k and φ_{k+1} , respectively, are:

$$f_{\varphi_k}(\alpha) = f_{\varphi_{k+1}}(\beta) = \begin{cases} \frac{1}{2\pi} & 0 \leq \alpha < 2\pi; 0 \leq \beta < 2\pi \\ 0 & \text{otherwise} \end{cases} \quad (3)$$

where α and β represent the values of φ_k and φ_{k+1} , respectively. The joint PDF of φ_k and φ_{k+1} is easily determined as follows:

$$f_{\varphi_k\varphi_{k+1}}(\alpha, \beta) = f_{\varphi_k}(\alpha) \cdot f_{\varphi_{k+1}}(\beta) = \begin{cases} \frac{1}{4\pi^2} & 0 \leq \alpha < 2\pi \text{ and } 0 \leq \beta < 2\pi \\ 0 & \text{otherwise} \end{cases} \quad (4)$$

The cumulative distribution function (CDF) $F_{\Delta\varphi_k}(\theta)$ of the phase difference $\Delta\varphi_k$ can be derived by the following integration (θ represents the value of $\Delta\varphi_k$):

$$F_{\Delta\varphi_k}(\theta) = P(\Delta\varphi_k \leq \theta) = \iint_{\substack{\beta - \alpha \leq \theta \\ 0 \leq \alpha < 2\pi \\ 0 \leq \beta < 2\pi}} f_{\varphi_k\varphi_{k+1}}(\alpha, \beta) d\alpha d\beta = \iint_{\substack{\beta - \alpha \leq \theta \\ 0 \leq \alpha < 2\pi \\ 0 \leq \beta < 2\pi}} \frac{1}{4\pi^2} d\alpha d\beta \quad (5)$$

The integral areas for $-2\pi < \theta \leq 0$ and $0 < \theta < 2\pi$ are shown in Figure 3a,b, respectively. When $-2\pi < \theta \leq 0$, the integral area takes the form of a triangle, whereas for $0 < \theta < 2\pi$, it manifests as a pentagon. In the case of $-2\pi < \theta \leq 0$, the CDF is derived by solving Equation (5) with the integral area shown in Figure 3a.

$$F_{\Delta\varphi_k}(\theta) = \int_0^{2\pi+\theta} \int_{\beta-\theta}^{2\pi} \frac{1}{4\pi^2} d\alpha d\beta = \frac{(2\pi + \theta)^2}{8\pi^2} \quad (6)$$

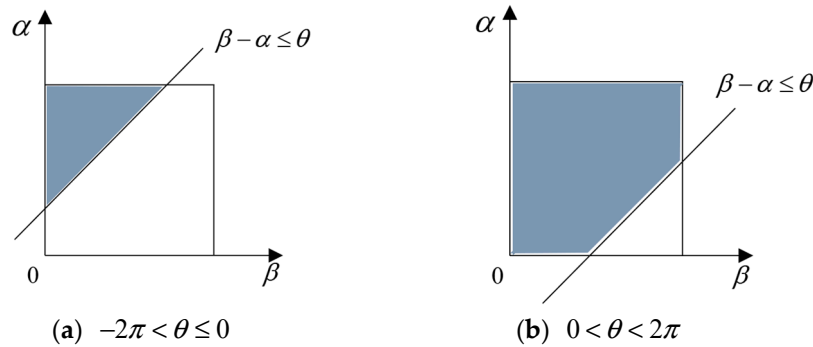


Figure 3. Integral areas of CDF of the phase difference $\Delta\varphi_k$.

Similarly, in the case of $0 < \theta < 2\pi$, considering Figure 3b, the CDF is:

$$F_{\Delta\varphi_k}(\theta) = \int_0^\theta \int_0^{2\pi} \frac{1}{4\pi^2} d\alpha d\beta + \int_\theta^{2\pi} \int_{\beta-\theta}^{2\pi} \frac{1}{4\pi^2} d\alpha d\beta = \frac{\theta}{2\pi} + \frac{4\pi^2 - \theta^2}{8\pi^2} \quad (7)$$

The CDF of the phase difference $\Delta\varphi_k$ is:

$$F_{\Delta\varphi_k}(\theta) = \begin{cases} \frac{(2\pi+\theta)^2}{8\pi^2} & -2\pi < \theta \leq 0 \\ \frac{\theta}{2\pi} + \frac{4\pi^2 - \theta^2}{8\pi^2} & 0 < \theta < 2\pi \end{cases} \quad (8)$$

Differentiating both sides of Equation (8) with regard to θ yields the PDF of $\Delta\varphi_k$:

$$f_{\Delta\varphi_k}(\theta) = \begin{cases} \frac{1}{2\pi} + \frac{\theta}{4\pi^2} & -2\pi < \theta \leq 0 \\ \frac{1}{2\pi} - \frac{\theta}{4\pi^2} & 0 < \theta < 2\pi \end{cases} \quad (9)$$

Equation (9) shows the PDF of the difference between two independent and uniformly distributed random variables. Evidently, the phase difference, $\Delta\varphi_k$, is triangularly distributed, as shown in Figure 4.

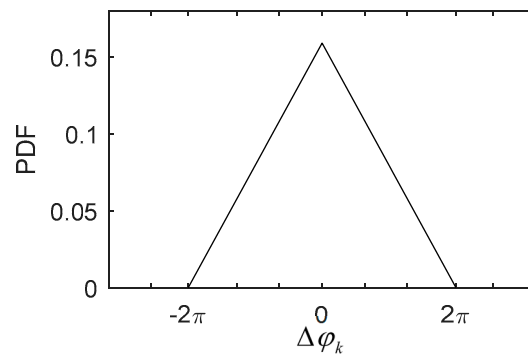


Figure 4. PDF of the difference between two independent and uniformly distributed random variables.

Furthermore, considering the periodicity of the phase differences (i.e., the fact that $\Delta\varphi_k$ changes in integer multiples of 2π has no influence), by adding 2π to each phase difference in the domain of $[-2\pi, 0)$, the phase difference can be changed to the domain of $[0, 2\pi)$. Thus, the PDF of the phase difference is simplified, as shown in Figure 5. The PDF of $[-2\pi, 0)$ translates 2π horizontally to the right. The sum of the translated and original PDFs of $[0, 2\pi)$, which are both indicated by solid lines in Figure 5a, is the final PDF of the phase difference, as shown by the solid line in Figure 5b. Thus, the PDF of the phase difference $\Delta\varphi_k$ in one period is:

$$f_{\Delta\varphi_k}(\theta) = \frac{1}{2\pi} \quad 0 \leq \theta < 2\pi \quad (10)$$

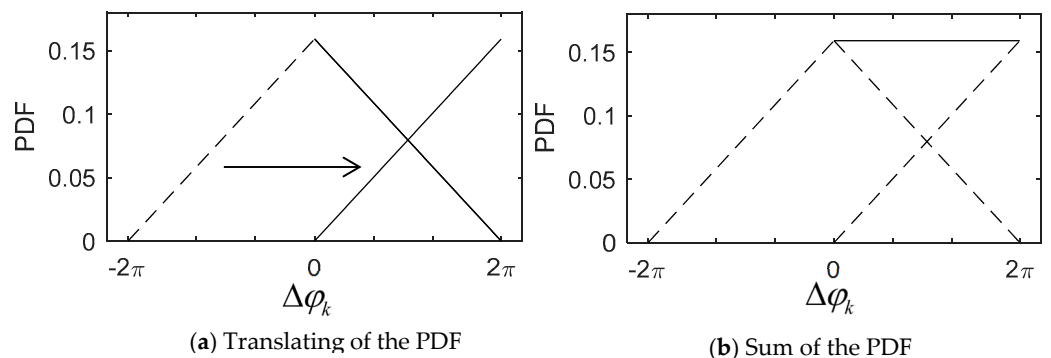


Figure 5. PDF of the phase difference $\Delta\varphi_k$.

As indicated by Equation (10), the phase difference $\Delta\varphi_k$ is uniformly distributed, which is contrary to the general knowledge that the phase difference follows a normal distribution. Therefore, the assumption that the phase angles are independent and uniformly distributed is not correct. Nevertheless, the probability distributions of the phase angles contained in the accelerograms of real earthquake ground motions seem to be uniform. Therefore, it can be deduced that the phase angles of real earthquake ground motions are uniformly distributed and correlated with each other.

The dependence of the phase angles indicates that they are dependent on the frequency or the Fourier amplitude. The first numerical experiment was conducted to further verify this dependence. The basic idea of the experiment was as follows.

If the phase angles are independent of each other, when they are in a different order, the time history will not change. In contrast, if a different time history is constructed when the phase angles are in a different order, the phase angles will be dependent on the frequency (or the Fourier amplitude), that is, the phase angles will correlate to each other.

In the first numerical experiment, a new phase spectrum was generated by changing only the order of the phase angles of the Parkfield-02,CA accelerogram. The new phase

spectrum and the original amplitude spectrum of the Parkfield-02,CA accelerogram were used to construct a new acceleration time history.

As shown in Figure 6, the newly constructed acceleration time history with out-of-order phase angles exhibits notable discrepancies compared to the original waveform, affecting various aspects such as the overall wave shape, detail of vibration, peak acceleration, and more. Notably, the non-stationarity of the earthquake ground motion underwent significant alterations, even when employing the same phase angles but in different orders, highlighting the interdependence of phase angles within real acceleration time histories. Furthermore, the findings from the numerical experiment underscore the profound impact of the phase spectrum on both the temporal shape and the time non-stationarity of ground motion.

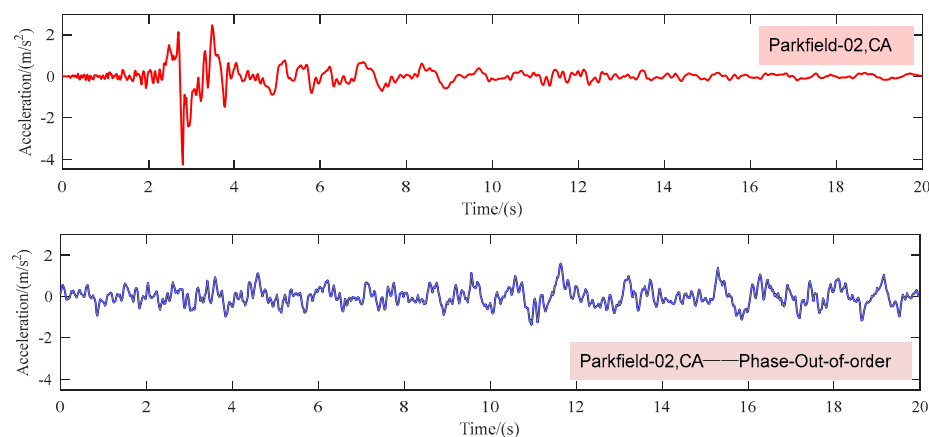


Figure 6. Original and new constructed Parkfield-02,CA acceleration time histories with out-of-order phase angles.

2.2. Probability Distribution of the Phase Differences

Because the phase angles of earthquake ground motion were correlated to each other, the phase differences of one accelerogram were deduced to be correlated to each other as well, based on Equation (2). Therefore, assuming that the phase differences are independent, normally distributed, or lognormally distributed is unreasonable. The second numerical experiment was conducted for further verification, whose basic idea was the same as that of the second numerical experiment.

The second numerical experiment: The out-of-order phase differences were obtained by changing the order of the phase differences of the Parkfield-02,CA accelerogram, while keeping the values unchanged. In sequence, the new phase spectrum was constructed utilizing the same initial phase angle of the Parkfield-02,CA accelerogram and out-of-order phase differences. The new phase spectrum and the original amplitude spectrum of the Parkfield-02,CA accelerogram were used to construct a new acceleration time history.

As shown in Figure 7, the newly constructed acceleration time history with the out-of-order phase differences was similar to the original Parkfield-02,CA accelerogram in the entire wave shape, but exhibited a large difference in the detail of vibration (particularly in the large pulse) and peak acceleration. The relative difference in the peak acceleration between the original and new acceleration time histories was as high as 17.65%. Thus, the phase differences of the real acceleration time history were correlated with each other. Furthermore, by comparing Figures 6 and 7, the out-of-order phase angles resulted in a larger difference to the acceleration time history than the out-of-order phase differences. It can be speculated that the dependence of the phase differences causes weaker differences in the acceleration time history than the dependence of the phase angles.

Based on the analysis of the probability distributions of the phase angles and the phase differences, as well as the results of the two numerical experiments, the preliminary conclusion was that the phase angles and phase differences were all dependent on the frequency (or the Fourier amplitude) and correlated to each other. Therefore, the genera-

tion of earthquake ground motions with independent and identically distributed phase differences without considering the dependences of phase differences is unreasonable.

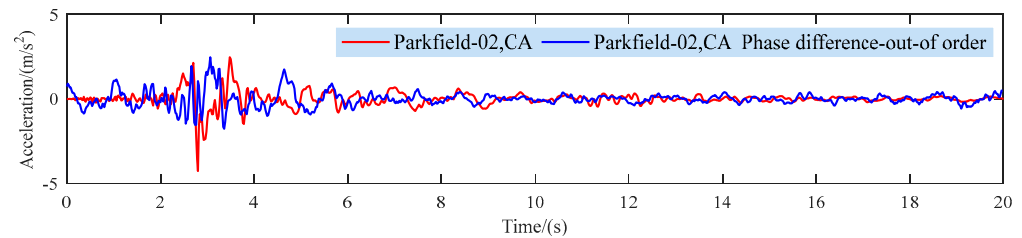


Figure 7. Original and newly constructed Parkfield-02,CA acceleration time histories with the out-of-order phase differences.

3. Physical Characteristics of the Phase Spectrum

The negative of the circular frequency-dependent phase derivative is called the envelope delay in physics and represents the delay time of the wave group at a certain frequency. In view of this envelope delay, the physical characteristics of the phase spectrum were studied.

3.1. Circular Frequency-Dependent Phase Derivative

A simple wave group is obtained when two waves with the same amplitude, but different frequencies (ω_1, ω_2) and phases (φ_1, φ_2), are superimposed, resulting in:

$$\begin{aligned}\psi &= A \cdot \cos(\omega_1 t + \varphi_1) + A \cdot \cos(\omega_2 t + \varphi_2) \\ &= 2A \cos(\Delta\omega t + \Delta\varphi) \cos(\omega t + \varphi)\end{aligned}\quad (11)$$

where

$$\omega = \frac{\omega_1 + \omega_2}{2}; \quad \varphi = \frac{\varphi_1 + \varphi_2}{2}; \quad \Delta\omega = \frac{\omega_2 - \omega_1}{2}; \quad \Delta\varphi = \frac{\varphi_2 - \varphi_1}{2}\quad (12)$$

Equation (11) represents a carrier with frequency ω and an envelope with frequency $\Delta\omega$, as shown in Figure 8. The wave may be described as a succession of wave groups (or wave packets).

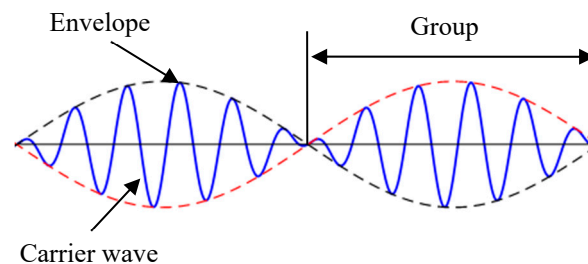


Figure 8. Superposition of two simple harmonic waves with the same amplitude.

Moreover, a more practical wave group, $a(t)$, is obtained when the simple harmonic waves in a narrow frequency band, $[\omega_0, \omega_0 + \Delta\omega]$, are superimposed, giving:

$$a(t) = \int_{\omega_0}^{\omega_0 + \Delta\omega} A(\omega) \cos[\omega t + \varphi(\omega)] d\omega\quad (13)$$

To simplify Equation (13), two assumptions were considered:

- (1) The amplitude $A(\omega)$ is a constant A_0 in $[\omega_0, \omega_0 + \Delta\omega]$, giving:

$$A(\omega) = A_0\quad (14)$$

- (2) The phase angle $\varphi(\omega)$ is approximated using Taylor's expansion in the neighborhood of ω_0 , in which only the first two terms are maintained, giving:

$$\varphi(\omega) = \varphi(\omega_0) + (\omega - \omega_0) \left. \frac{d\varphi}{d\omega} \right|_{\omega=\omega_0} = \varphi_0 + (\omega - \omega_0) \left. \frac{d\varphi}{d\omega} \right|_{\omega=\omega_0} \quad (15)$$

Substituting Equations (14) and (15) into Equation (13) and evaluating the integral yields:

$$\begin{aligned} a(t) &= A \frac{\sin \xi}{\xi} \Delta\omega \cos(\omega_0 t + \varphi_0 + \xi) \\ &= F(\xi) \cos(\omega_0 t + \varphi_0 + \xi) \end{aligned} \quad (16)$$

where:

$$F(\xi) = A \Delta\omega \frac{\sin \xi}{\xi} \quad (17)$$

$$\xi = \frac{\Delta\omega}{2} \left(t + \left. \frac{d\varphi}{d\omega} \right|_{\omega=\omega_0} \right) \quad (18)$$

Equation (16) includes two parts that are similar to Equation (11). This equation also represents a carrier wave with frequency ω_0 and an envelope, $F(\xi)$. A typical envelope is illustrated in Figure 9, in which the negative of the circular frequency-dependent phase derivative is the time delay of the amplitude of the envelope, namely the envelope delay, as follows:

$$t_e = - \left. \frac{d\varphi}{d\omega} \right|_{\omega=\omega_0} \quad (19)$$

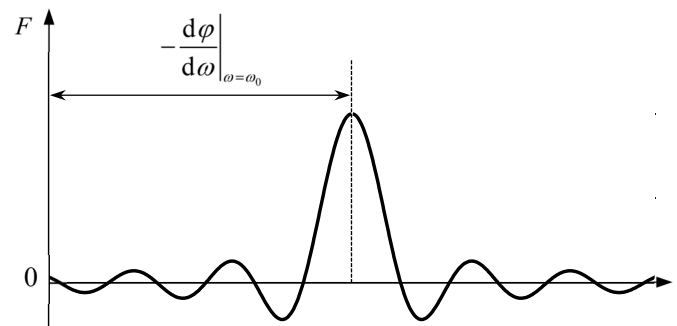


Figure 9. Typical envelope of the wave group in a narrow band.

Specifically, the envelope delay of earthquake ground motion is the time delay of the amplitude envelopes of the various cosine components of a time history recorded at a specified site and is a function of frequency for each component. Because the envelope delay represents the time delay of each component of the time history, it is easily determined that:

$$t_e = - \left. \frac{d\varphi}{d\omega} \right|_{\omega=\omega_0} \in [0, T] \quad (20)$$

where T is the total duration of the time history.

By introducing the concept of equivalent group velocity and assuming that the source of the earthquake is a point, Jin and Liao [24] deduced that the negative of the circular frequency-dependent phase derivative denotes the envelope delay of the wave group with a certain circular frequency to the site with respect to the fastest wave group. In view of this, the time delay corresponding to the amplitude of the narrowband wave group (envelope delay) is defined as the arrival time of the wave group. Thus, the time history of the earthquake ground motion is a result of the superposition of the wave groups arriving at different times. This conclusion was drawn based on the two abovementioned assumptions. Because the assumptions hold only when the bandwidth, $\Delta\omega$, is sufficiently small, the stable wave group can be generated only in a sufficiently narrow frequency band.

Wave propagation is the propagation of energy by nature, and the propagation of energy is the propagation of the amplitude of a wave with a fixed frequency [42]. Therefore, the envelope delay of any stable wave group in the frequency band is sufficiently narrow and is the arrival time of the amplitude as well as the energy.

For the discrete time history of earthquake ground motions, the envelope delay is:

$$t_e(\omega_k) = -\frac{\Delta\varphi(\omega_k)}{\Delta\omega} \quad (21)$$

where $\Delta\omega = 2\pi/T$. When $\Delta\varphi \in (-2\pi, 0]$, $t_e \in (0, T]$ satisfies the definition of the envelope delay of the wave group. Consequently, the phase difference in this study has a range:

$$\Delta\varphi \in (-2\pi, 0] \quad (22)$$

3.2. Relation of the Envelope Delay and Fourier Amplitudes

Because the envelope delay, t_e , is linear to the phase difference, $\Delta\varphi$, according to Equation (21), the relation between the Fourier amplitudes and the envelope delays is similar to that of the Fourier amplitudes and the phase differences. Three accelerograms were chosen to analyze the relation between the Fourier amplitudes and the envelope delays. Detailed information on the three accelerograms is presented in Table 1. The scatter diagrams of the envelope delays and Fourier amplitudes are shown in Figure 10.

Table 1. Information of the accelerograms used in the numerical cases in Section 3.2.

No.	Earthquake	Date	Magnitude	Station Name/Code	Azimuth
1	Chi-Chi	20 September 1999	7.62	HWA041	EW
2	Big Bear-01	28 June 1992	6.46	LA-1955 1/2 Purdue Ave. Bsmt	235°
3	Wenchuan	12 May 2008	8.0	051AXT	NS

The envelope delays spread out over different ranges corresponding to different Fourier amplitudes, which is similar to the relation of the phase differences and Fourier amplitudes [22]. In contrast to the scatter diagram of phase differences and the Fourier amplitudes, the envelope delays have units of time between zero and the duration of the earthquake ground motion. As shown in Figure 10, the three selected accelerations differ in duration and exhibit distinct occurrence times of strong shocks. However, despite these differences, wave groups with larger amplitudes arrived at approximately the same time at which a strong shock occurred for all three accelerations. For instance, the strong shock of the Chi-Chi accelerogram occurred at approximately 50 s, and the wave groups with large amplitudes arrived around the same time. Conversely, the amplitudes of wave groups during the initial and attenuation stages are considerably smaller. Similarly, in the Big Bear-01 accelerogram, a pronounced shock can be observed between 20 s and 30 s, during which wave groups with larger amplitudes arrive within the same time range. Moreover, amplitudes of wave groups outside this time range are notably smaller. In contrast to the aforementioned earthquakes, the Wenchuan earthquake had two strong shocks due to its unique source mechanism: the stronger one occurred around 50 s and the weaker one between 100 s and 150 s. According to the scatter diagram of the Wenchuan accelerogram, wave groups with large amplitudes arrived at approximately 50 s and 125 s. Similarly, amplitudes of wave groups outside these time ranges are notably smaller. The envelope delays for tens of thousands of accelerograms were analyzed and showed this tendency.

The relation between the Fourier amplitudes and the envelope delays provides strong evidence of the definition of the envelope delay, which denotes the arrival time of the wave group, and proves that $\Delta\omega = 2\pi/T$ is reasonable. The non-stationary characteristics of ground motion in the time domain stem from variations in the arrival times of wave groups with different amplitudes. This variability primarily results from the nonuniformity of fault rupture.

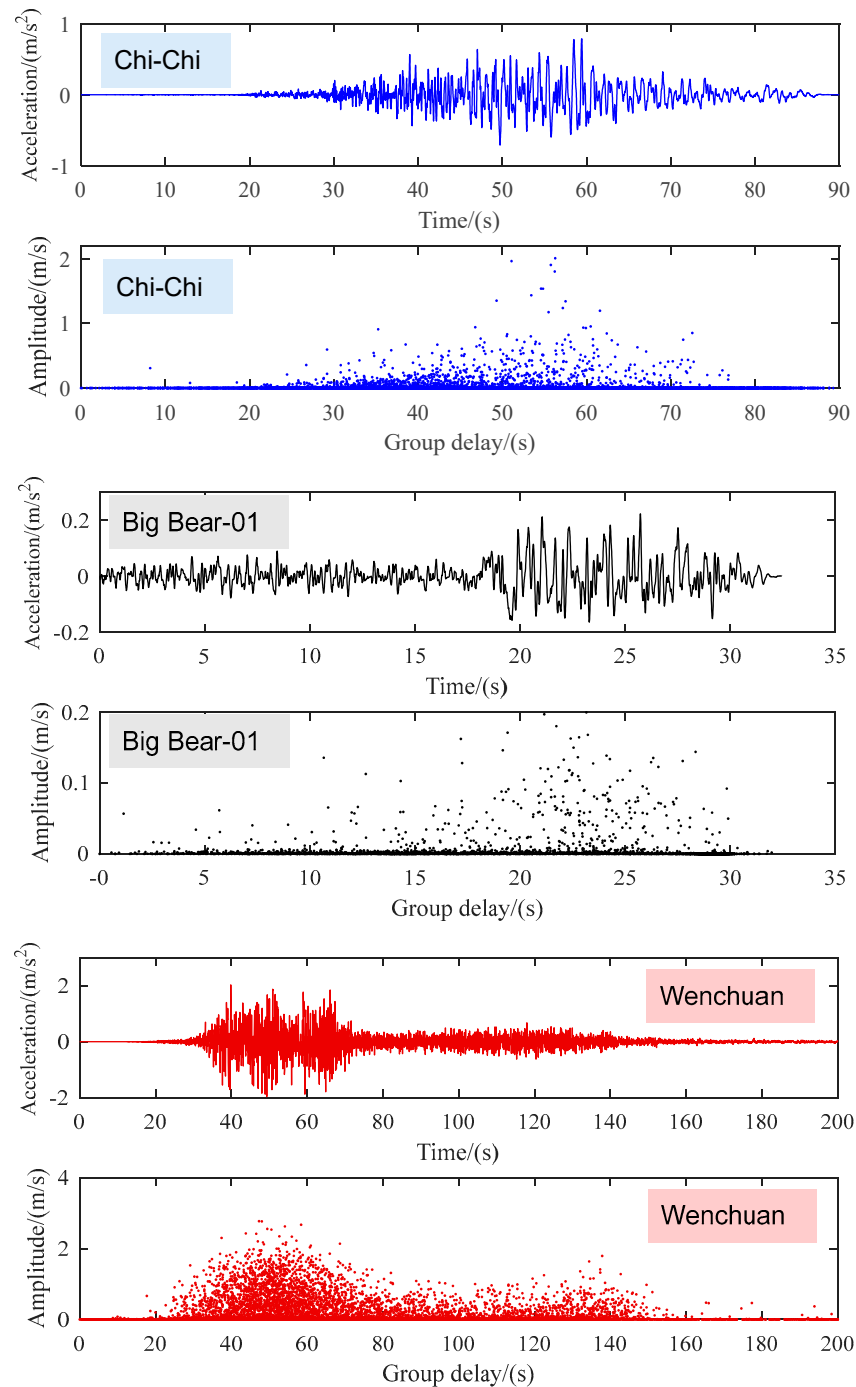


Figure 10. Scatter diagrams of the envelope delays and amplitudes.

As indicated in Sections 3.1 and 3.2, the time property, which is the essential characteristic of the phase spectrum, was revealed. The arrival times of the wave groups were included in the phase spectrum, which was the reason for the generation of different time histories when the order of the phase differences was changed, as indicated by the results of the second numerical experiment. The arrival times of the wave groups changed when the order of the phase differences was changed, which resulted in a different time history of the earthquake ground motion.

4. Influence of the Source, Propagation Path, and Site on the Phase Spectrum

The significant influence of earthquake acceleration by the source, propagation path, and site has been demonstrated [43,44]. In this study, the wave groups versus different

frequencies arrive at different times. This is because the occurrence time and propagation velocities of the wave groups are different, which is related to the fault rupture and propagation of earthquake waves. In this section, the influence of the source, propagation path, and site on the phase spectrum is analyzed to investigate the mechanism of the time property of the phase spectrum.

4.1. Data

Five earthquake accelerograms (see Data and Resources Section) were chosen to illustrate the influence of the source, propagation path, and site on the phase spectrum. The locations of the epicenters and stations are shown in Figure 11, and the detailed information of the five accelerograms is listed in Table 2. Accelerograms No. 1 and No. 2 were both from the Chi-Chi earthquake and recorded in ILA067 and TAP081 stations, respectively. As shown in Figure 11, the epicenters of the Chi-Chi earthquake, ILA067 station, and TAP081 station were approximately in a straight line. The v_{s30} of accelerogram No. 1 was the same as that of accelerogram No. 3; the epicentral distance of the accelerogram No. 2 was twice that of accelerogram No. 1. Hence, accelerograms Nos. 1 and 2 were used to analyze the influence of the propagation path because they were almost the same in both the source and site. Accelerograms Nos. 1 and 3 were recorded from the Chi-Chi earthquake and its aftershock, respectively; therefore, their sources were very close to each other. Because they were recorded at the same station, they were almost the same in the propagation path and site. Therefore, accelerograms Nos. 1 and 3 were used for the analysis of the source. Accelerograms Nos. 4 and 5 were both from the Wenchuan earthquake; their observation stations had the same longitude and latitude but different elevations: one was on the bedrock and the other was on the ground. Therefore, they were the same in the source and propagation paths and were used for the analysis of the site.

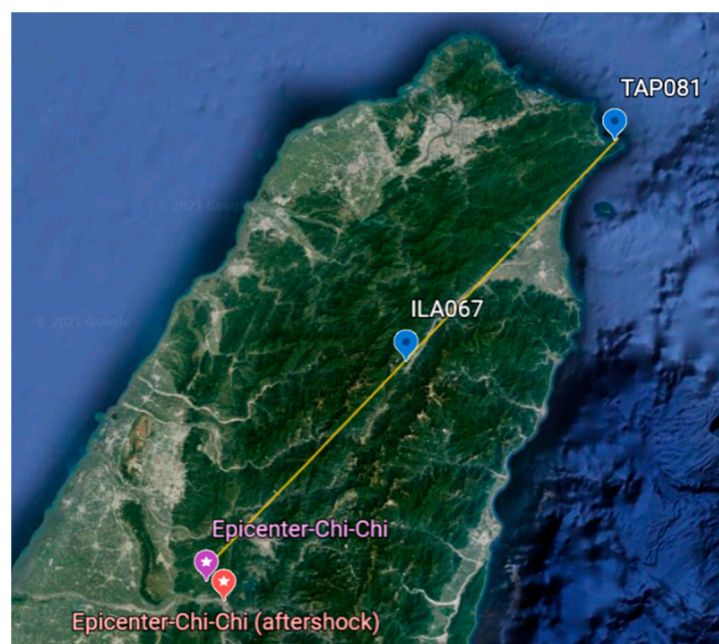


Figure 11. Location of epicenters and stations of Nos. 1, 2, and 3 in Table 2.

Table 2. Information of earthquake accelerograms used in Section 4.

No.	Earthquake	Magnitude	Date	Epicenter		No.	Station		Azimuth	Epicentral Distance (km)	Site Condition	v_{s30} (m/s)
				Latitude	Longitude		Latitude	Longitude				
1	Chi-Chi	7.62	20 September 1999	23.86	120.80	ILA067	24.44	121.37	EW	86.38	Soil	553.4
2	Chi-Chi	7.62	20 September 1999	23.86	120.80	TAP081	25.02	121.98	EW	175.3	Soil	553.4
3	Chi-Chi (aftershock)	6.2	20 September 1999	23.81	120.85	ILA067	24.44	121.37	EW	87.94	Soil	553.4
4	Wenchuan	8.0	12 May 2008	31.00	103.40	51BXZ	30.50	102.90	EW	--	Rock	--
5	Wenchuan	8.0	12 May 2008	31.00	103.40	51BXY	30.50	102.90	EW	--	Soil	--

4.2. Influence of the Source

Accelerograms Nos. 1 and 3 are shown in Figure 12, along with their frequency distribution histograms and scatter diagrams of the envelope delays. Comparing Figure 12a,b, a considerable difference in the duration and wave shape between the two accelerograms can be observed; the envelope delays of accelerogram No. 3 are distributed more dispersedly than those of accelerogram No. 1. As shown in the scatter diagram of the envelope delays, the envelope delays of accelerogram No. 1 versus frequencies lower than 50 Hz are considerably more concentrated than those for frequencies higher than 50 Hz, whereas the envelope delays are dispersedly distributed at all frequencies for accelerogram No. 3. The envelope delays exhibited a significant difference when the two accelerograms were almost the same in the propagation path and in the site soil. This means that the source had a significant influence on the phase spectrum.

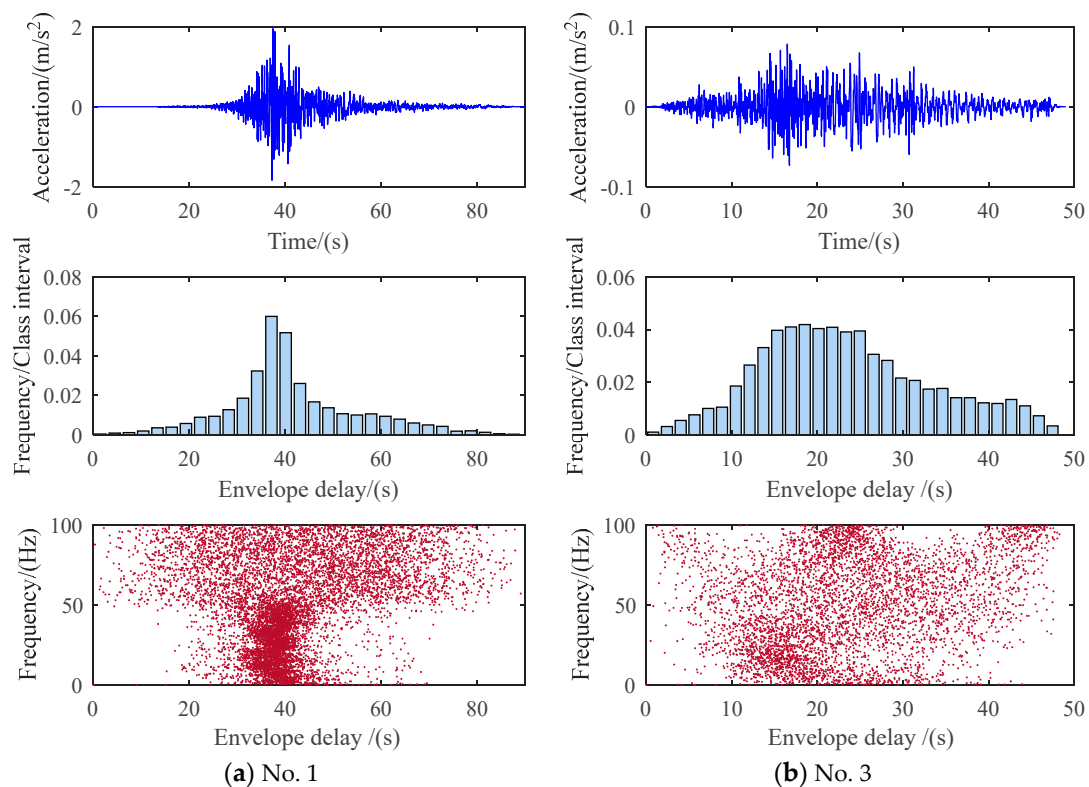


Figure 12. Accelerograms, frequency distribution histograms, and scatter diagrams of the envelope delays of Nos. 1 and 3 in Table 2.

Evidently, the arrival time of the wave group was partly determined by the occurrence time, which was determined by the size of the fault and velocity of the rupture. Therefore, the envelope delay was influenced by the fault rupture process. Thus, to summarize, the time heterogeneity of the energy release of the fault rupture was one of the key reasons for the complex distribution of envelope delays.

4.3. Influence of the Propagation Path

Accelerograms Nos. 1 and 2 are shown in Figure 13, along with their frequency distribution histograms and scatter diagrams of the envelope delays. Comparing Figure 13a,b, it can be observed that the duration of accelerogram No. 1 is close to that of accelerogram No. 2, and they have similar wave shapes; however, there is a large difference in the distribution of the envelope delays. The envelope delays of accelerogram No. 2 are dispersedly distributed at all frequencies, as well as those of accelerogram No. 3. The envelope delays of the two records show a significant difference when the two accelerograms are almost

the same in the source and in the site soil. This means that the propagation path had a significant influence on the phase spectrum.

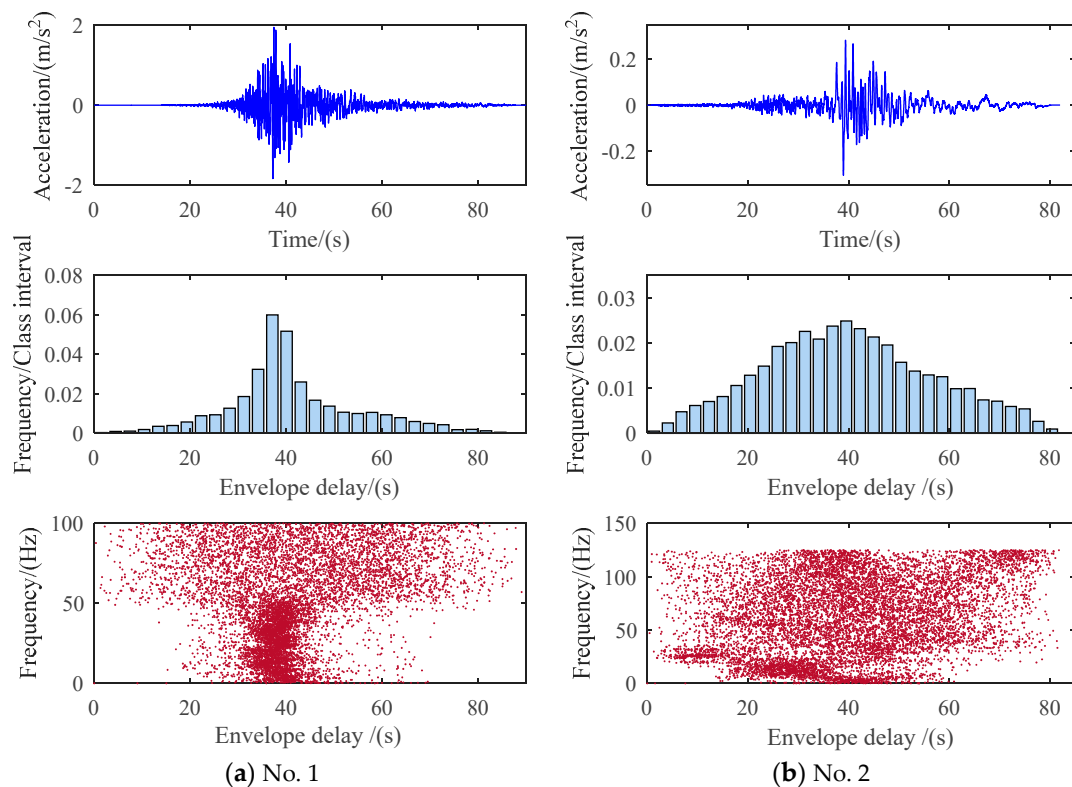


Figure 13. Accelerograms, frequency distribution histograms, and scatter diagrams of the envelope delays of Nos. 1 and 2 in Table 2.

As shown in Figure 11, the earthquake wave of the Chi-Chi earthquake started from the source and propagated to station ILA067, and accelerogram No. 1 was first recorded. The earthquake wave moved ahead toward station TAP081. In this process, the earthquake waves with different frequencies propagated at different velocities, caused by the dispersion of earthquake waves and resulting in different propagation time delays, even at the same distance. One extreme case is that all the wave groups arrived at station ILA067 at the same time, and the wave groups were dispersed when reached station TAP081 as a result of the dispersion of the earthquake waves. It is inferred that the longer the propagation distance, the more dispersed the wave groups for an earthquake wave. Therefore, we can conclude that the dispersion of the earthquake wave was the other key reason for the complex distribution of envelope delays.

4.4. Influence of the Site

Accelerograms Nos. 4 and 5 are shown in Figure 14, along with their frequency distribution histograms and scatter diagrams of the envelope delays. As shown in Figure 14, these accelerograms have almost the same duration. Although the frequency distribution histograms of the envelope delays show some differences, their shapes are similar to each other. The wave groups of high frequency recorded in the rock (No. 4) arrived at three times, whereas the arrival time of that recorded in the soil (No. 5) was considerably more dispersed. This indicates that the soil influenced the phase spectrum. That is, the dispersion of the earthquake wave at the site had an influence on the phase spectrum. However, the influence of the site on the phase spectrum was smaller with respect to the source and path because the propagation distance at the site was much smaller.

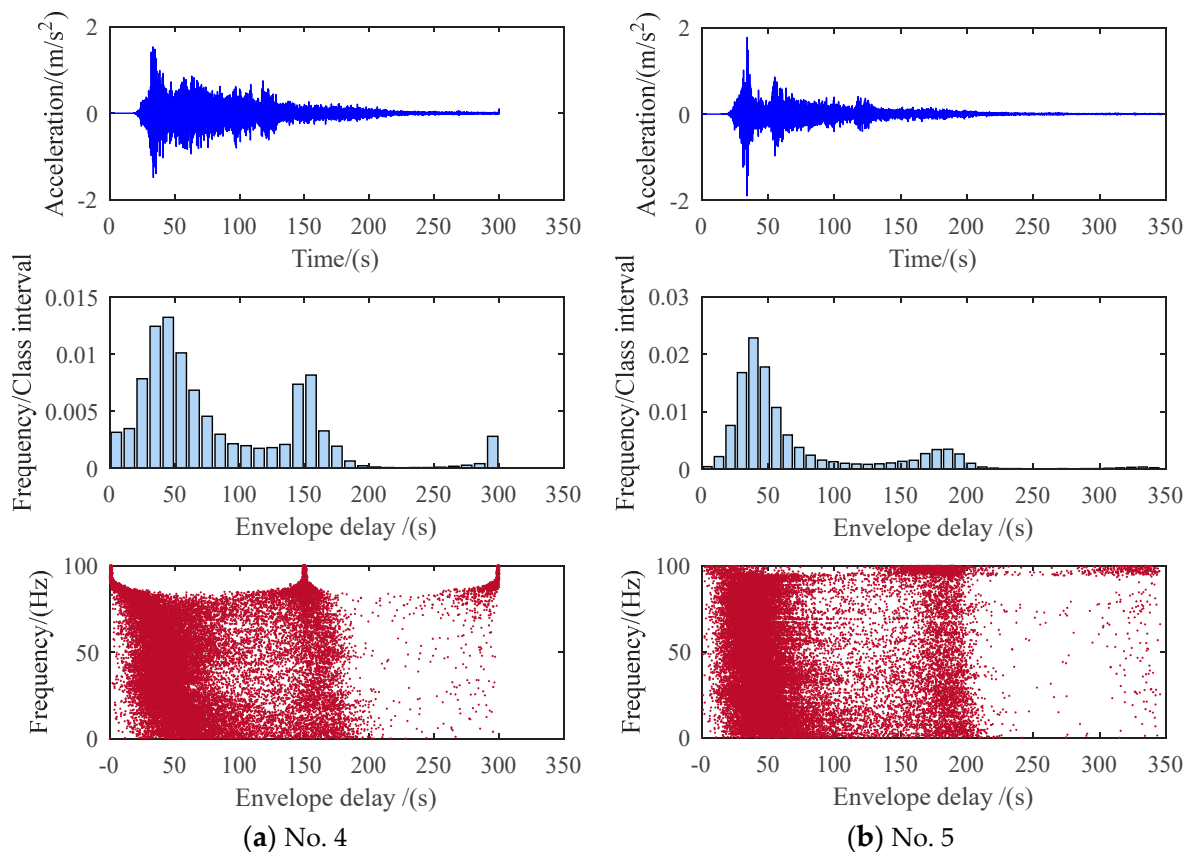


Figure 14. Accelerograms, frequency distribution histograms, and scatter diagrams of the envelope delays of Nos. 4 and 5 in Table 2.

Finally, we can conclude that the phase spectrum of earthquake ground motion is mainly affected by the source and path, and the source has the most important role. The influence of the site is smaller and can be neglected to some extent.

5. Conclusions and Discussion

Through an examination of the mathematical characteristics of phase angles and phase differences of earthquake ground acceleration time history, this study provides insights into the phase spectrum. Contrary to previous assumptions, phase angles cannot be considered uniformly and independently distributed random variables. Our analysis reveals that phase angles of earthquake ground acceleration time history exhibit correlation and approximate a uniform distribution over one period. Similarly, phase differences of earthquake ground acceleration time history display a correlation and appear to follow a normal distribution within one period. Consequently, generating ground motions based on independently distributed phase differences is deemed unreasonable. The identification of correlations among phase angles and phase differences represents a noteworthy discovery in this investigation. It introduces a novel perspective for comprehending the mathematical characteristics of the phase spectrum of earthquake ground motions.

The physical attributes of the phase spectrum of earthquake ground motions were determined using the envelope delay, which signifies the arrival time of wave groups. The fundamental physical characteristic of the phase spectrum, namely its temporal properties, was demonstrated. Further investigation into the influence of source, propagation path, and site on the phase spectrum reveals that the temporal heterogeneity in the energy release during the fault rupture and dispersion of earthquake waves are the primary contributors to the complex temporal properties of the phase spectrum.

The results of this study indicate that the dependences of phase angles, as well as phase differences, result from the physical process of the occurrence and propagation

of earthquake waves. The time heterogeneity of the fault rupture and the dispersion in propagation result in specific distributed envelope delays and complex characteristics of the phase spectrum. The presented research introduces a novel concept for simulating the phase spectrum of ground motion. It is anticipated that this innovation will pave the way for the development of a time-frequency non-stationary ground motion simulation method rooted in the phase spectrum rather than a time modulation function.

Author Contributions: Conceptualization, Y.D. and H.M.; Data curation, Y.D.; Formal analysis, Y.X.; Funding acquisition, Y.D.; Investigation, Y.D. and H.M.; Methodology, Y.D. and Y.X.; Project administration, Y.D.; Resources, Y.D. and Y.X.; Software, Y.D.; Supervision, Y.D. and H.M.; Validation, H.M.; Visualization, Y.D.; Writing—original draft, Y.D.; Writing—review and editing, Y.X. and H.M. All authors have read and agreed to the published version of the manuscript.

Funding: This research was funded by the National Natural Science Foundation of China (Grant No. 52008339) and China Postdoctoral Science Foundation (Grant No. 2022MD723815).

Data Availability Statement: All the accelerograms of the Wenchuan earthquake used in this study were provided by the China Strong Motion Network Centre at Institute of Engineering Mechanics, China Earthquake Administration. The other data were download from the website of <http://ngawest2.berkeley.edu/> (accessed on 20 January 2024).

Acknowledgments: The support of the National Natural Science Foundation of China and China Postdoctoral Science Foundation is also appreciated. The authors are also grateful to the China Strong Motion Network Centre at Institute of Engineering Mechanics, China Earthquake Administration and the Pacific Earthquake Engineering Research Center for providing the earthquake ground motions.

Conflicts of Interest: The authors declare no conflicts of interest.

References

1. Sertel, E. Identification of Earthquake Induced Damage Areas Using Fourier Transform and SPOT HRVIR Pan Images. *Sensors* **2009**, *9*, 1471–1484. [[CrossRef](#)] [[PubMed](#)]
2. Madariaga, R.; Ruiz, S.; Rivera, E.; Leyton, F.; Baez, J.C. Near-field spectra of large earthquake. *Pure Appl. Geophys.* **2019**, *176*, 983–1001. [[CrossRef](#)]
3. Cho, I.H. Sharpen data-driven prediction rules of individual large earthquakes with aid of Fourier and Gauss. *Sci. Rep.* **2023**, *13*, 16009. [[CrossRef](#)] [[PubMed](#)]
4. Boore, D.M. Simulation of ground motion using the stochastic method. *Pure Appl. Geophys.* **2003**, *160*, 635–676. [[CrossRef](#)]
5. Rezaeian, S.; Der Kiureghian, A. A stochastic ground motion model with separable temporal and spectral nonstationarities. *Earthq. Eng. Struct. Dyn.* **2008**, *37*, 1565–1584. [[CrossRef](#)]
6. Wang, D.; Li, J. Physical random function model of ground motions for engineering purposes. *Sci. China Technol. Sci.* **2011**, *54*, 175–182. [[CrossRef](#)]
7. Kanai, K. Semi-empirical formula for the earthquake characteristics of the ground. *Bull. Earthq. Res. Inst. Univ. Tokyo Jpn.* **1957**, *35*, 309–325.
8. Tajimi, H. A statistical method of determining the maximum response of a building structure during an earthquake. In Proceedings of the 2th World Conference on Earthquake Engineering, Tokyo, Japan, 11–18 July 1960.
9. Clough, R.W.; Penzien, J. *Dynamics of Structures*; McGraw-Hill Book Co.: New York, NY, USA, 1975.
10. Oppenheim, A.V.; Lim, J.S. The importance of phase in signals. *Proc. IEEE* **1981**, *69*, 529–541. [[CrossRef](#)]
11. Yegnanarayana, B.; Saikia, D.; Krishnan, T. Significance of group delay functions in signal reconstruction from spectral magnitude or phase. *IEEE Trans. Acoust. Speech Signal Process.* **1984**, *32*, 610–623. [[CrossRef](#)]
12. Shi, G.; Shanechi, M.M.; Aarabi, P. On the importance of phase in human speech recognition. *IEEE Trans. Audio Speech Lang. Process.* **2006**, *14*, 1867–1874.
13. Skarbnik, N.; Zeevi, Y.Y.; Sagiv, C. *The Importance of Phase in Image Processing*; Faculty of Electrical Engineering, Technion-Israel Institute of Technology: Haifa, Israel, 2009.
14. Kakarala, R. A signal processing approach to Fourier analysis of ranking data: The importance of phase. *IEEE Trans. Signal Process.* **2011**, *59*, 1518–1527. [[CrossRef](#)]
15. Bakulin, A.; Silvestrov, I.; Neklyudov, D. Importance of phase guides from beamformed data for processing multi-channel data in highly scattering media. *J. Acoust. Soc. Am.* **2020**, *147*, EL447–EL452. [[CrossRef](#)] [[PubMed](#)]
16. Shinozuka, M. Simulation of multivariate and multidimensional random processes. *J. Acoust. Soc. Am.* **1971**, *49*, 357–368. [[CrossRef](#)]
17. Shinozuka, M.; Deodatis, G. Simulation of stochastic processes by spectral representation. *Appl. Mech. Rev.* **1991**, *44*, 191–204. [[CrossRef](#)]

18. Liu, Z.; Liu, W.; Peng, Y. Random function based spectral representation of stationary and non-stationary stochastic processes. *Probabilistic Eng. Mech.* **2016**, *45*, 115–126. [[CrossRef](#)]
19. Sarkar, K.; Gupta, V.K.; George, R.C. Wavelet-based generation of spatially correlated accelerograms. *Soil Dyn. Earthq. Eng.* **2016**, *87*, 116–124. [[CrossRef](#)]
20. Chen, J.; Kong, F.; Peng, Y. A stochastic harmonic function representation for non-stationary stochastic processes. *Mech. Syst. Signal Process.* **2017**, *96*, 31–44. [[CrossRef](#)]
21. Ohsaki, Y. On the significance of phase content in earthquake ground motions. *Earthq. Eng. Struct. Dyn.* **1979**, *7*, 427–439. [[CrossRef](#)]
22. Nigam, N.C. Phase properties of a class of random processes. *Earthq. Eng. Struct. Dyn.* **1982**, *10*, 711–717. [[CrossRef](#)]
23. Sawada, T. Application of phase differences to the analysis of nonstationarity of earthquake ground motion. In Proceedings of the 8th World Conference on Earthquake Engineering, Prentice Hall, New York, NY, USA, 21–28 July 1984.
24. Jin, X.; Liao, Z. Relation between envelope function of strong ground motions and frequency number distribution function of phase difference spectrum. *Earthq. Eng. Eng. Vib.* **1990**, *10*, 20–26. (In Chinese)
25. Thráinsson, H.; Kiremidjian, A.S. Simulation of digital earthquake accelerograms using the inverse discrete Fourier transform. *Earthq. Eng. Struct. Dyn.* **2002**, *31*, 2023–2048. [[CrossRef](#)]
26. Montaldo, V.; Kiremidjian, A.S.; Thráinsson, H.; Zonno, G. Simulation of the Fourier phase spectrum for the generation of synthetic accelerograms. *J. Earthq. Eng.* **2003**, *7*, 427–445. [[CrossRef](#)]
27. Nagao, K.; Kanda, J. Study of a Ground-Motion Simulation Method using a Causality Relationship. *J. Earthq. Eng.* **2014**, *18*, 891–907. [[CrossRef](#)]
28. Han, X.; Wang, Z.; Peng, L.; Su, J.; Wang, L. Numerical Simulation of Seismic Waves with Peak Arrival Time and Amplitude-Frequency Correlation. *KSCE J. Civ. Eng.* **2019**, *23*, 4389–4406. [[CrossRef](#)]
29. Zhu, Y.; Feng, Q. Distribution characteristic of phase difference spectrum and artificial accelerogram. *Earthq. Eng. Eng. Vib.* **1992**, *12*, 37–44.
30. Zhang, C.; Sato, T.; Lu, L. A phase model of earthquake motions based on stochastic differential equation. *KSCE J. Civ. Eng.* **2011**, *15*, 161–166. [[CrossRef](#)]
31. Sato, T. Fractal characteristics of phase spectrum of earthquake motion. *J. Earthq. Tsunami* **2013**, *7*, 1350010. [[CrossRef](#)]
32. Baglio, M.G. Stochastic Ground Motion Method Combining a Fourier Amplitude Spectrum Model from a Response Spectrum with Application of Phase Derivatives Distribution Prediction. Ph.D. Thesis, Politecnico di Torino, Turin, Italy, 2017.
33. Ding, Y.; Peng, Y.; Li, J. A stochastic semi-physical model of seismic ground motions in time domain. *J. Earthq. Tsunami* **2018**, *12*, 1850006. [[CrossRef](#)]
34. Lavrentiadis, G.; Abrahamson, N. Generation of surface-slip profiles in the wavenumber domain. *Bull. Seism.-Log. Soc. Am.* **2019**, *109*, 888–907. [[CrossRef](#)]
35. Han, X.; Liu, Y.; Wang, L. The normal distribution fitting method for frequency distribution characteristics of peak arrival time of earthquake. *Adv. Compos. Lett.* **2020**, *29*, 2633366X20921411. [[CrossRef](#)]
36. Wang, H.; Wang, F.; Yang, H.; Feng, Y.; Bayless, J.; Abrahamson, N.A.; Jeremić, B. Time domain intrusive probabilistic earthquake risk analysis of nonlinear shear frame structure. *Soil Dyn. Earthq. Eng.* **2020**, *136*, 106201. [[CrossRef](#)]
37. Boore, D.M. Phase derivatives and simulation of strong ground motions. *Bull. Seismol. Soc. Am.* **2003**, *93*, 1132–1143. [[CrossRef](#)]
38. Ding, Y.Q.; Peng, Y.B.; Li, J. Physically based phase spectrum and simulation of strong earthquake ground motions. In Proceedings of the 16th World Conference on Earthquake Engineering, Santiago, Chile, 9–13 January 2017.
39. Li, L.; Silva-Castro, J. Synthesis of single-hole signatures by group delay for ground vibration control in rock blasting. *J. Vib. Control* **2020**, *26*, 1273–1284. [[CrossRef](#)]
40. Dai, M.; Li, Y.; Dong, Y. Incorporation of envelope delays and amplifications into simulation of far-field long-period ground motions. *Soil Dyn. Earthq. Eng.* **2020**, *136*, 106192. [[CrossRef](#)]
41. Kumari, N.; Gupta, I.D.; Sharma, M.L. Synthesizing nonstationary earthquake ground motion via empirically simulated equivalent group velocity dispersion curves for Western Himalayan region. *Bull. Seismol. Soc. Am.* **2018**, *108*, 3469–3487. [[CrossRef](#)]
42. Liao, Z. *Introduction to Wave Motion Theories in Engineering*, 2nd ed.; Science Press: Beijing, China, 2002.
43. El-Nabulsi, R.A.; Anukool, W. Fractal dimension modeling of seismology and earthquakes dynamics. *Acta Mech.* **2022**, *233*, 2107–2122. [[CrossRef](#)]
44. Perez, J.S.; Llamas, D.C.; Buhay, D.J.; Constantino, R.C.; Legaspi, C.J.; Lagunsad, K.D.; Grutas, R.N.; Quimson, M.M. Impacts of a Moderate-Sized Earthquake: The 2023 Magnitude (Mw) 4.7 Leyte, Leyte Earthquake, Philippines. *Geosciences* **2024**, *14*, 61. [[CrossRef](#)]

Disclaimer/Publisher’s Note: The statements, opinions and data contained in all publications are solely those of the individual author(s) and contributor(s) and not of MDPI and/or the editor(s). MDPI and/or the editor(s) disclaim responsibility for any injury to people or property resulting from any ideas, methods, instructions or products referred to in the content.